Ultracompact and fabrication-tolerant integrated polarization splitter

A. Hosseini,[1,2] S. Rahimi,[1] X. Xu,[1] D. Kwong,[1] J. Covey,[1] and R. T. Chen[1,3]

[1]*Microelectronic Research Center, Department of Electrical and Computer Engineering, University of Texas at Austin, 10100 Burnet Rd. Austin, TX 78758 USA*

[2]*e-mail: amirh@utexas.edu*

[3]*e-mail: raychen@uts.cc.utexas.edu*

Received July 26, 2011; revised September 5, 2011; accepted September 5, 2011; posted September 19, 2011 (Doc. ID 151611); published October 12, 2011

Design and fabrication of a 2 × 2 two-mode interference (TMI) coupler based on-chip polarization splitter is presented. By changing the angle between the access waveguides, one can tune the effective TMI length for the mode with less optical confinement (transverse magnetic, TM) to coincide with the target TMI length for a desired transmission of the mode with higher optical confinement (transverse electric, TE). The fabricated 0.94 μm long 2 × 2 TMI splits the input power into TM (bar) and TE (cross) outputs with splitting ratio over 15 dB over 50 nm bandwidth. Fabrication tolerance analysis shows that the device is tolerant to fabrication errors as large as 60 nm. © 2011 Optical Society of America

OCIS codes: 130.3120, 130.2790.

On-chip polarization splitters (PSs) are key components of integrated photonic circuits that consist of polarization-dependent devices [1]. Interference-based passive PSs provide low-loss operation and high polarization splitting ratio (SR) and can be designed for single etch step fabrication [2]. The interference-based PSs that have been demonstrated thus far utilize either directional couplers [2,3] or multimode-interference couplers (MMIs) [4,5].

Symmetric directional coupler based PSs can be shortened (~100 μm) by reducing the gap between the coupled waveguides [3]. However, this also degrades the device fabrication tolerance and potentially lowers its SR. Non-symmetric directional couplers can be designed to allow only one of the modes (TE or TM) to couple out of the input waveguide. The device fabrication tolerance can be improved by waveguide tapering [2]. However, this technique assumes linear design conditions that require relatively large gaps and thus, due to long coupling lengths, the resulting devices are ~1500 μm long [2].

In MMI based PSs, TM and TE polarizations can be split into different bar or cross states using the difference in their self-imaging beat-lengths, $L_\pi = \pi/(\beta_0 - \beta_1)$, where β_n is the nth mode propagation constant supported by the multimode section [6]. In order to avoid long MMIs due to small beat-length differences of TM and TE polarizations, the required MMI length can be shortened by use of four-mode interference couplers [4], and further by use of two-mode interference (TMI) couplers [5].

In order for a TMI to function as a polarization splitter, the TMI length (L_{TMI}) is chosen to be simultaneously equal to an odd (even) multiple of L_π for the TE polarization (L_π^{TE}) and an even (odd) multiple of L_π for the TM polarization (L_π^{TM}). A PS device on silicon-on-insulator (SOI) with L_{TMI} (not including the access waveguides) as short as 8.8 μm has been demonstrated [5]. However, the resulting TMI is still several beat-lengths long. Since the fabrication tolerance and optical bandwidth of MMI devices are inversely proportional to their length [7], it is beneficial to reduce the TMI length to its absolute minimum, one beat-length. In this Letter, we report the design and fabrication of a one-beat-length long TMI based PS.

A schematic of the proposed TMI based PS on SOI is shown in Fig. 1(a). The thicknesses of the oxide and top silicon layers (h) are 3 μm and 230 nm, respectively. A TMI width 800 nm $< W_{\mathrm{TMI}} <$ 950 nm supports only two TE and two TM modes, suitable for TMI operation [8]. The input/output access waveguide width is $W_w = W_{\mathrm{TMI}}/2$. For a TMI, the output power at port 3 and 4 normalized to input power at port 1 (port 2 is idle) is given as $P_3/P_1 = \sin^2(\pi L_{\mathrm{TMI}}/2L_\pi + \varphi)$ and $P_4/P_1 = \cos^2(\pi L_{\mathrm{TMI}}/2L_\pi + \varphi)$, where, the phase term, φ, is determined by the coupling between the two access waveguides at the input and output. Assuming fixed h, only W_{TMI} and L_{TMI} have been thus far considered as the design parameters while the effect of φ on the device operation has been ignored.

Assuming $W_{\mathrm{TMI}} = 900$ nm, $h = 230$ nm, and wavelength, $\lambda = 1550$ nm, we simulate the device in Fig. 1(a) using the full vectorial eigenmode decomposition-based complex film mode matching (FMM) solver (with 60 1D modes) of the FIMMPROP module. Figure 1(b) shows the variations of power splitting ratio, $P4/P3$ and $P3/P4$, versus L_{TMI} for input TE and TM polarizations, respectively. One notes that φ depends on both polarization and the angle between the access waveguides, θ. Also, for a

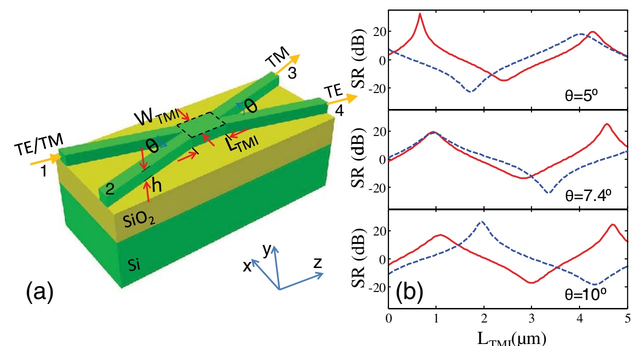

Fig. 1. (Color online) (a) Schematic of the polarization splitter device. (b) Variations of P4/P3 and P3/P4 for input TE (solid red line) and TM (dashed blue line) polarized light, respectively, at different θ values, for $W_{\mathrm{TMI}} = 900$ nm and $h = 230$ nm at $\lambda = 1550$ nm.

 © 2011 Optical Society of America

TM-polarized input, a change in θ has a considerably large effect on φ. This is not surprising, as the TM mode supported by the access waveguides is much less confined compared to the TE mode. Thus, for a TM input, the coupling between the two access waveguides is considerably stronger resulting in an effectively larger $L_{\rm TMI}$ that is more sensitive to θ than that for a TE input. Since the power splitting ratio changes much slowly with θ for a TE-polarized input, the easily tunable θ can be used as a reliable design parameter for tuning the output SR.

Figure 1(b) shows that at $\theta = 7.4°$ and $L_{\rm TMI} = 0.94\,\mu$m, the 2×2 PS device operates in the cross and bar states for TE- and TM-polarized inputs, respectively. Note that $L_{\rm TMI} = 0.94\,\mu$m is shorter than both $L_\pi^{\rm TE} = 1.80\,\mu$m and $L_\pi^{\rm TM} = 2.31\,\mu$m. Figure 2 shows the field propagation through this device from finite-difference time-domain (FDTD) (RSoft™) simulations, which indicate that at $\theta = 7.4°$, $L_{\rm TMI} = 0.94\,\mu$m effectively corresponds to $2L_\pi^{\rm TM}$ and $1L_\pi^{\rm TE}$. SR values for TE and TM inputs are $P4/P3 = 19.4$ dB and $P3/P4 = 18.6$ dB, respectively. Insertion loss values for TE and TM inputs are $P3/P1 = -0.25$ dB and $P4/P1 = -0.35$ dB, respectively.

Based on our simulation results the device performance becomes independent of the input/output access waveguide length when they are longer than $6.5\,\mu$m. Thus, the total device length, including the input/output access waveguides, is $13.94\,\mu$m. Ultracompact directional coupler based PSs with similar dimensions have been reported [9,10]. As discussed before, the fabrication tolerance remains an issue for short directional couplers with small gap sizes. In order to investigate the proposed PS fabrication tolerance, we assume that the fabrication errors appear as changes in waveguide width (ΔW) [2].

The device layout changes due to $\Delta W < 0$ and $\Delta W > 0$ are depicted in Fig. 3(a) inset. A $\Delta W < 0$ does not change the TMI length while widening the gap between the access waveguides. When the waveguide width increases ($\Delta W > 0$), one can imagine that the *effective* TMI length increases but the *effective* gap between the access waveguides is just shifted away from the original TMI.

Variations of insertion loss and SR with ΔW for TE- and TM-polarized inputs are shown in Figs. 3(a) and 3(b), respectively. TM mode propagation in the access waveguides is near the mode cutoff, and a reduction in the waveguide width ($\Delta W < 0$) results in a significantly less confined modal field. Thus, in the case of TM input, the effect of wider gap due to $\Delta W < 0$ is compensated by the stronger coupling between the more spread-out modal fields. As the coupling at the access waveguides does not play a significant role for TE polarization, the PS

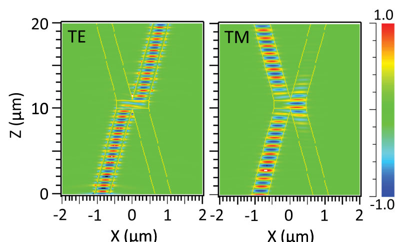

Fig. 2. (Color online) FDTD Propagation field profiles for TE (Ex) and TM (Hx) input polarizations for $\theta = 7.4°$, $L_{\rm TMI} = 940$ nm, $W_{\rm TMI} = 900$ nm, and $h = 230$ nm at $\lambda = 1550$ nm.

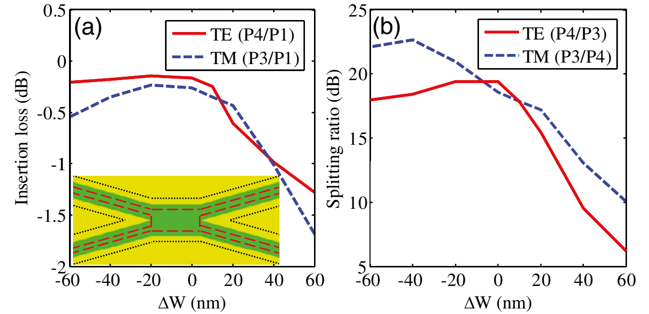

Fig. 3. (Color online) Variations of (a) insertion loss and (b) polarization splitting ratio as functions of deviation in the waveguide width for input TE and TM polarizations. The inset of (a) shows a PS layout affected by $\Delta W < 0$ (dashed red) and $\Delta W > 0$ (dotted black).

device is tolerant to $\Delta W < 0$ for both TE and TM polarizations.

On the other hand, a $\Delta W > 0$ effectively increases the TMI length as $\Delta L = \Delta W/\sin(\theta/2) = 15.5\Delta W$. In other words, $\Delta L/L \approx 15\Delta W/W$. Note that for the self-imaging process in the TMI to be tolerant to small changes in the TMI width, the changes in the (effective) TMI length must satisfy $\Delta L/L = 2\Delta W/W$ [7]. Therefore, the large changes in the MMI length rapidly degrade the TMI performance for $\Delta W > 10$ nm, for both TE- and TM-polarized inputs in a similar way. Note that for $\Delta W < 0$, the device fabrication tolerance is comparable to that of a tapered asymmetric directional coupler, which is nearly 500 times larger [2].

To benefit from tolerance to $\Delta W < 0$, we choose a fabrication process with a possible shrinkage in the waveguide width. For $\Delta W < 0$, the minimum distance between the access waveguides on each side is given as $\Delta W \cos(\theta)$. For $\Delta W < 0$, the tip shape between the access waveguides is blunt and does not introduce fabrication difficulties. The PS device is fabricated on Soitec SOI wafers consisting of three micron thick silicon dioxide and 250 nm thick top silicon device layer. The top silicon layer is oxidized to create a 45 nm top silicon dioxide layer, which serves as a hard mask in the silicon etch process.

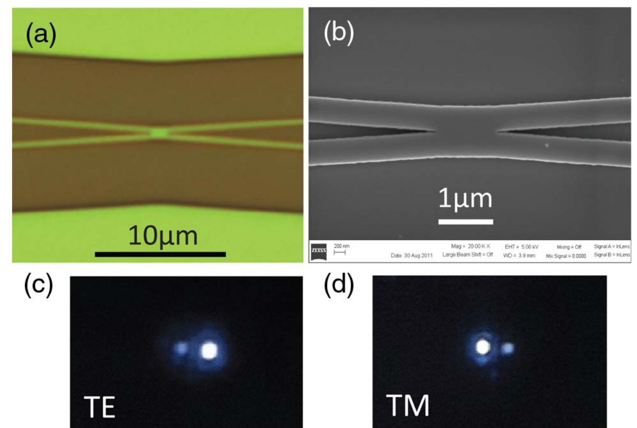

Fig. 4. (Color online) (a) Microscope and (b) SEM images of the fabricated PS device. Top-down IR pictures of the PS outputs for (c) TE and (d) TM polarized inputs.

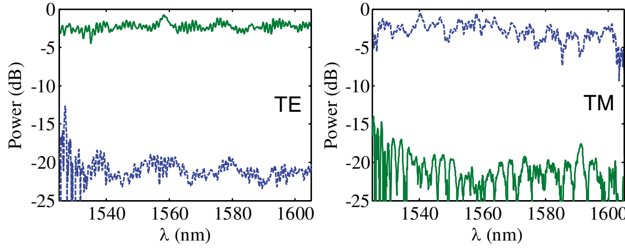

Fig. 5. (Color online) Normalized output transmission spectra at P3 (dashed blue) and P4 (solid green) for TE and TM input excitations at P1. Data is normalized to the measured ASE output spectrum.

The oxidation process consumes 20 nm of the top silicon layer and results in a final 230 nm silicon layer. The top oxide layer is patterned using electron beam lithography and CHF3/O2 plasma based reactive ion etching (RIE). The pattern is then transferred to the silicon layer underneath by HBr/Cl2 based RIE. In addition to a small etch undercut, due to the E-beam proximity effect, the area of the exposed positive resist (ZEP520) expands a little bit resulting in narrowing of the unetched areas of the top silicon layer. Overall, with this fabrication process, $\Delta W < 0$ is expected. Microscope and SEM images of the fabricated PS are shown in Fig. 4. Top-down SEM measurements indicate a final $\Delta W = -20$ nm.

The PSs are tested on a Newport six-axis autoaligning station. A broadband amplified spontaneous emission (ASE) source output light, covering $1520 \sim 1620$ nm, is TE- or TM-polarized with an extinction ratio of over 30 dB and butt coupled into/out of the input/output waveguide facets through a polarization maintaining lensed fiber. Top-down IR pictures of the outputs at the chip edge with TE- and TM-polarized input excitations are shown in Fig. 4.

Figure 5 shows the spectra of normalized output power measured at Port 3 and Port 4, for TE and TM input excitations at Port 1. The results indicate polarization splitting ratios of $P4/P3 = 18.2$ dB and $P3/P4 = 16.8$ dB, respectively, for the TE- and TM-polarized inputs at $\lambda = 1550$ nm. The splitting ratio remains better than 15 dB over a 70 nm bandwidth for the TE-polarized input and over 50 nm bandwidth for the TM-polarized input. The TE and TM propagation losses in a fabricated $450\ \text{nm} \times 230\ \text{nm}$ waveguide are estimated to be 7.5 dB/cm and 16.3 dB/cm, respectively, using a cutback technique, at $\lambda = 1550$. In order to accurately estimate the device insertion loss, while excluding the input/output fiber/waveguide coupling loss and propagation losses in the access waveguides, we compare the transmission through two-stage cascaded TMIs with the transmission through a single TMI for each polarization. A narrowband laser ($\lambda = 1550$) is used for insertion loss measurements. Our results indicate that the insertion loss is 0.8 dB for the TE-polarized input and 1.7 dB for the TM-polarized input.

In summary, we presented the design and fabrication of a TMI based PS, for which the length of the TMI section is reduced to less than a single beat-length of the TE mode. While the device performance is sensitive to the angle between the two input/output access waveguides, the device is rather tolerant to width variations (shrinkage) in the TMI and the access waveguides. To the best of our knowledge, this TMI is the most compact and largest bandwidth self-imaging device demonstrated so far.

This research is supported by the multidisciplinary university research initiative (MURI) program through the United States Air Force Office of Scientific Research (USAFOSR), contract no. FA 9550-08-1-0394.

References

1. S. Corzine, P. Evans, M. Fisher, J. Gheorma, M. Kato, V. Dominic, P. Samra, A. Nilsson, J. Rahn, I. Lyubomirsky, A. Dentai, P. Studenkov, M. Missey, D. Lambert, A. Spannagel, S. Murthy, E. Strzelecka, J. Pleumeekers, A. Chen, R. Schneider, R. Nagarajan, M. Ziari, J. Stewart, C. Joyner, F. Kish, and D. Welch, IEEE Photon. Technol. Lett. **22**, 1015 (2010).
2. L. M. Augustin, J. J. G. M. van der Tol, R. Hanfoug, W. J. M. de Laat, M. J. E. van de Moosdijk, P. W. L. van Dijk, Y.-S. Oei, and M. K. Smit, J. Lightwave Technol. **25**, 740 (2007).
3. I. Kiyat, A. Aydinli, and N. Dagli, IEEE Photon. Technol. Lett. **17**, 100 (2005).
4. J. M. Hong, H. H. Ryu, S. R. Park, J. W. Jeong, S. G. Lee, E.-H. Lee, S.-G. Park, D. W. Woo, S. Kim, and B.-H. O, IEEE Photon. Technol. Lett. **15**, 72 (2003).
5. B.-K. Yang, S.-Y. Shin, and D. Zhang, IEEE Photon. Technol. Lett. **21** (7), 432 (2009).
6. D. M. Mackie, T. J. Tayag, and T. E. Batchman, Opt. Eng. **40**, 2265 (2001).
7. P. A. Besse, M. Bachmann, H. Melchior, L. B. Soldano, and M. K. Smit, J. Lightwave Technol. **12**, 1004 (1994).
8. F. Rottmann, A. Neyer, W. Mevenkamp, and E. Voges, J. Lightwave Technol. **6**, 946 (1988).
9. H. Fukuda, K. Yamada, T. Tsuchizawa, T. Watanabe, H. Shinojima, and S. Itabashi, Opt. Express **14**, 12401 (2006).
10. S. Lin, J. Hu, and K. Crozier, Appl. Phys. Lett. **98**, 151101 (2011).